

Article

# Catalytic Oxidation of Benzyl Alcohol Using Nanosized Cu/Ni Schiff-Base Complexes and Their Metal Oxide Nanoparticles

Sameerah I. Al-Saeedi <sup>1</sup>, Laila H. Abdel-Rahman <sup>2,\*</sup>, Ahmed M. Abu-Dief <sup>2</sup>,  
Shimaa M. Abdel-Fatah <sup>2</sup>, Tawfiq M. Alotaibi <sup>3</sup>, Ali M. Alsalmeh <sup>4</sup> and Ayman Nafady <sup>4,\*</sup>

<sup>1</sup> Department of Chemistry, College of Science, Princess Nourah bint Abdulrahman University, Riyadh 11451, Saudi Arabia; sialsaeedi@pnu.edu.sa

<sup>2</sup> Chemistry Department, Faculty of Science, Sohag University, Sohag 82534, Egypt; ahmed.benzoic@yahoo.com (A.M.A.-D.); shimaamahdy80@yahoo.com (S.M.A.-F.)

<sup>3</sup> King Abdullah City for Atomic and Renewable Energy, Riyadh 11451, Saudi Arabia; tawfiq377@hotmail.com

<sup>4</sup> Chemistry Department, College of Science, King Saud University, Riyadh 11451, Saudi Arabia; aalsalmeh@ksu.edu.sa

\* Correspondence: lailakenawy@hotmail.com (L.H.A.R.); anafady@ksu.edu.sa (A.N.); Tel.: +966-569-407-110 (A.N.)

Received: 26 September 2018; Accepted: 10 October 2018; Published: 13 October 2018



**Abstract:** In this work, nanosized Cu and Ni Schiff-base complexes, namely ahpvCu, ahpnbcu, and ahpvNi, incorporating imine ligands derived from the condensation of 2-amino-3-hydroxypyridine, with either 3-methoxysalicylaldehyde (ahpv) or 4-nitrobenzaldehyde (ahpnb), were synthesized using sonochemical approach. The structure and properties of the new ligands and their complexes with Ni(II) and Cu(II) were determined via infrared (IR), nuclear magnetic resonance (NMR), electronic spectra (UV-Vis), elemental analysis (CHN), thermal gravimetric analysis (TGA), molar conductivity ( $\Lambda_m$ ), and magnetic moment ( $\mu_{\text{eff}}$ ). The combined results revealed the formation of 1:1 (metal: ligand) complexes for ahpvCu and ahpvNi and 1:2 for ahpnbcu. Additionally, CuO and NiO nanoparticles were prepared by calcination of the respective nanosized Cu/Ni complexes at 500 °C, and characterized by powder X-ray diffraction (XRD) and transmission electron microscopy (TEM). Significantly, the as-prepared nanosized Schiff-base Cu/Ni complexes and their oxides showed remarkable catalytic activity towards the selective oxidation of benzyl alcohol (BzOH) in aqueous H<sub>2</sub>O<sub>2</sub>/dimethylsulfoxide (DMSO) solution. Thus, catalytic oxidation of BzOH to benzaldehyde (BzH) using both ahpvCu complex and CuO nanoparticles in H<sub>2</sub>O<sub>2</sub>/DMSO media at 70 °C for 2 h yielded 94% and 98% BzH, respectively, with 100% selectivity.

**Keywords:** Schiff-base Cu(II) and Ni(II) complexes; metal oxides; nanoparticles; sonochemical; catalytic activity; benzyl alcohol

## 1. Introduction

Owing to their wide-spread application in biology, biomedicine, and catalysis, complexes bearing Schiff-base ligands are among the most intensively explored coordination compounds [1–4]. A large number of Schiff-base transition-metal complexes are commonly employed as oxidation catalysts in a variety of important organic transformations, because of their facile synthesis and excellent chemical and thermal stability [2,5–8]. Given their inherent conducting and magnetic properties, Schiff-base complexes are also employed as precursors in many technologies, including electrochromic display screens, organic batteries, and microelectronic devices [9–13].

Selective oxidation of alcohols to aldehydes is an important and widely used reaction, as aldehydes are crucial intermediates for many organic syntheses and essential precursors for making vitamins,

drugs, and fragrances. Benzaldehyde (BzH), in particular, is commonly employed in the manufacture of flavors, odorants, and other pharmaceutical products [14–18]. Previous studies have shown that manipulation of the reaction conditions (e.g., reactant concentration, temperature, and pressure) and the choice of solvent and oxidation catalyst are essential factors for controlling the reaction rate, along with the nature and quantity of the generated side products [17,19]. However, in view of their pivotal role in redox chemistry, tremendous efforts have been devoted in recent years to design and develop novel types of catalysts to improve the selectivity and chemical yield of such reactions [15,16,20,21].

Among the endeavors in the exploration of smart materials in catalysis, inorganic precursors, such as metal oxides (MOs) have received considerable interest over the past few decades, due to their ability to withstand extremely harsh reaction conditions and their promising catalytic activity toward many important transformation processes [21–27]. The catalytic properties of these metal oxides rely, in part, on their high surface area and the relative acidity and basicity of the atoms present on their surface, which can be tuned via coordination of metal cations and oxygen anions [28–31]. However, the great challenge in the synthesis of nanotechnology-based materials lies in the production of nanostructures with desired properties that can be tailored and/or tuned to meet specific applications [32–37].

In this contribution, we explored the catalytic activity of nanosized Ni(II) and Cu(II) complexes comprising Schiff-base ligands derived from the condensation of 2-amino-3-hydroxypyridine with 3-methoxysalicylaldehyde or 4-nitrobenzaldehyde along with their generated MO nanoparticles (MO = NiO and CuO) [1] on the oxidation of benzyl alcohol (BzOH) under homogeneous conditions. Other experimental parameters, such as the effect temperature, concentration, and various solvents on the catalytic oxidation of BzOH, were also investigated. Our findings revealed that the parent complexes together with their respective MO showed efficient catalytic activity for oxidation of BzOH into BzH with approximately 100% selectivity under mild conditions.

## 2. Results and Discussion

### 2.1. Physicochemical Characteristics

All the prepared complexes are hydrated, air-stable solids at ambient temperature. The physicochemical and analytical results of Schiff-base ligands and their M(II)-complexes (M = Cu and Ni) are described in details in Table S1 in the Supplementary Materials. Complexes ahpvCu and ahpvNi display a 1:1 (metal: ligand) ratio, whereas the ahpnbCu complex presents a 1:2 stoichiometry (vide infra).

### 2.2. <sup>1</sup>H-NMR Spectroscopy

The <sup>1</sup>H-NMR spectra of the prepared Schiff-base ahpv and ahpnb ligands in dimethylsulfoxide (DMSO)-*d*<sub>6</sub> show a singlet signal at 9.44 and 9.39 ppm for the azomethine (CH=N) proton, multiple signals at 6.85–8.00 and 7.25–8.46 for six and seven aromatic protons. Moreover, the ahpnb ligand displays only a singlet signal at 10.28 for the OH proton, whereas the ahpv ligand shows similar singlet signal at 10.23 and 6.41 for the OH protons in the pyridine ring and adjacent to OCH<sub>3</sub>, respectively, along with a singlet signal at 3.34 for the three OCH<sub>3</sub> protons [1,38,39].

### 2.3. Infrared and Electronic Spectra

The characteristic infrared (IR) frequencies of the ligands and their complexes, together with their assignments, are shown in Table S2. The bands assigned to –OH and –CH=N groups are distinguishable and provide insight into the structure of the ligands and their bonding to the metal ion. The bands at 1613 and 1621 cm<sup>–1</sup> in the ahpv and ahpnb ligands, respectively, are attributed to the –C=N stretching vibration. Upon coordination, these bands shift to lower wavenumbers by 5–12 cm<sup>–1</sup>. This negative shift is indicative of the direct coordination of the azomethine nitrogen atoms to the metal ion [1,40,41]. This conclusion is supported by the appearance of strong bands within 527–656 cm<sup>–1</sup> range, corresponding to the stretching of the M–N bond.

Additionally, the IR bands at 3447 and 3475 cm<sup>–1</sup> observed for both ahpv and ahpnb ligands are consistent with the stretching vibration of free –OH. The IR spectra of all the prepared complexes show

broad bands at 3450 and 3490  $\text{cm}^{-1}$ , assigned to the  $\nu(\text{OH})$  stretching vibration of the hydrated water molecules in the complexes, as evidenced by the elemental analysis data listed in Table S1. However, the observation of IR bands at 814–976  $\text{cm}^{-1}$  (OH rocking) implies the existence of coordinated  $\text{H}_2\text{O}$  in the prepared complexes. The Schiff-base (ahpv and ahpnb) ligands also display absorption bands at 1307 and 1288  $\text{cm}^{-1}$ , respectively, which are assigned to the stretching vibration of the phenolic C–O group. The shift of that band to lower wavenumbers by 9–35  $\text{cm}^{-1}$  for ahpv and 3  $\text{cm}^{-1}$  for ahpnb upon complexation implies that the oxygen atoms of deprotonated phenolic groups are directly coordinated to the metal ion. The involvement of such bands in binding to the metal ion is further supported by the appearance of strong non ligand bands within 723–736  $\text{cm}^{-1}$  range, assigned to the stretching vibration of the M–O bond. As reported for related complexes, the bands observed in the region of 3047–3079  $\text{cm}^{-1}$  are assigned to  $\nu(\text{C-H})$  aromatic stretching vibrations [1,42].

Figure S1 showed representative electronic absorption spectra of the ahpvCu complex and its components in *N,N'*-dimethylformamide (DMF) in the wavelength range of 200–800 nm at 25 °C. The absorption bands below 300 nm are assigned to  $\pi\text{-}\pi^*$  transitions in the aromatic rings, whereas the absorption bands at  $\lambda_{\text{max}} = 314\text{--}349$  nm are attributed to  $n\text{-}\pi^*$  transitions of the imine group in the Schiff-base ligands [43]. As for the complexes, the absorption bands at  $\lambda_{\text{max}} = 239\text{--}391$  nm are consistent with a charge transfer in the Schiff-base ligands [44], whereas the broad bands at  $\lambda_{\text{max}} = 430\text{--}506$  nm are indicative of d–d transitions in the complexes [44].

#### 2.4. Magnetic Moment Measurements and Thermal Analysis

Magnetic susceptibility provides valuable insights on the geometric structure of compounds. In this context, the magnetic susceptibility results (Table S1) revealed that all prepared complexes exhibit paramagnetism and octahedral geometry, except for the ahpvCu complex, which presents a tetrahedral geometry [45]. The thermal behavior of the as-prepared complexes revealed the loss of the hydrated water molecules in the first step; then, in subsequent steps, the coordinated water molecules are released and the ligands decomposed, as shown in Table S3 [46]. The final decomposition products were identified as the metallic species [47,48].

#### 2.5. Spectrophotometric Determination of the Stoichiometry of the Prepared Complexes

The stoichiometry of the prepared Schiff-base complexes was determined using two spectrophotometric methods, namely, the continuous variation and molar ratio methods [49]. The curves obtained from the continuous variation method revealed a maximum absorbance at a mole fraction  $X_{\text{ligand}} = 0.43\text{--}0.68$ , thereby suggesting metal-to-ligand complexation in a molar ratio of either 1:1 or 1:2, as illustrated in Figure 1a. Similarly, the results obtained from the molar ratio method supported the above findings for the three prepared complexes, as shown in Figure 1b. Consistent with the aforementioned characterization, the data obtained from the two methods clearly confirm that the stoichiometry (metal: ligand) is 1:1 for both ahpvCu and ahpvNi complexes, and 1:2 for the ahpnbCu congener.

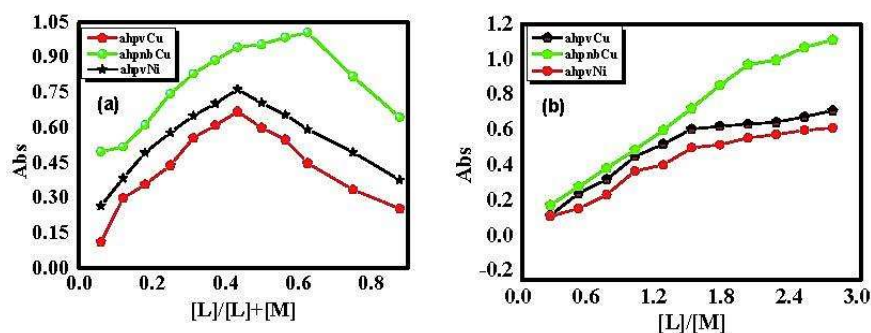


**Figure 1.** (a) Continuous variation, and (b) molar ratio plots for the prepared complexes in aqueous ethanolic solution at  $[M] = [L] = 1 \times 10^{-3}$  M and 298 K.

## 2.6. Formation Constants and pH Stability Range of the Complexes

The formation constant ( $K_f$ ) of the prepared Schiff-base Cu- and Ni-complexes in solution was determined via spectrophotometric measurements using the continuous variation method and Equation (1) [50]:

$$K_f = \frac{A/A_m}{4C_2(1 - A/A_m)^3}, \quad (1)$$

where  $A_m$  is the absorption at the maximum formation of the complex,  $A$  denotes arbitrary absorbance values on either side of the absorbance curve, and  $C$  is the elementary concentration of the metal. As summarized in Table 1, the obtained  $K_f$  values reflect the high stability of the prepared complexes. Importantly, the negative values of the Gibbs free energy ( $\Delta G^\ddagger$ ) mean that the reactions are spontaneous and favorable.

**Table 1.** Formation constant ( $K_f$ ), stability constant (pK), and Gibbs free energy ( $\Delta G^\ddagger$ ) values of the synthesized complexes in aqueous ethanol at 298 K.

Complex	Stoichiometry	$K_f$	pK	$\Delta G^\ddagger$ (kJ mol <sup>-1</sup> )
ahpvCu	1:1	$7.15 \times 10^8$	8.85	-50.48
ahpnbCu	1:2	$3.62 \times 10^{10}$	10.55	-60.20
ahpvNi	1:1	$9.60 \times 10^9$	9.98	-56.91

Furthermore, the pH profiles (absorbance vs. pH, Figure S2) of the prepared complexes established their marked stability in a wide pH range (4–11). This behavior indicates that the stability of the Schiff-base ligands is strongly enhanced by formation of the corresponding complexes, thereby making them suitable for various applications (vide infra).

## 2.7. Particle Size of the Prepared Complexes and Their Metal Oxides

Cu(II) and Ni(II) oxide nanoparticles were synthesized at 500 °C using the Schiff-base complexes as precursors and their structure and morphology were examined by transmission electron microscopy (TEM) and powder X-ray diffraction (PXRD). Based on the TEM images and the calculated histograms (Figure 2), it is evident that the prepared complexes have an average particle size of 46 and 65 nm, for ahpvCu and ahpvNi, respectively. The corresponding metal oxides (CuO and NiO) have a particle size of 42 and 16 nm as illustrated in Figure S3. These results clearly confirm that the prepared compounds have high surface area, which is essential for application in catalysis, as discussed in details below [51].

The X-ray diffraction (XRD) patterns of the synthesized CuO and NiO nanoparticles, as shown in Figure 3. The obtained XRD data are consistent with the reported values for CuO and NiO, thereby confirming the formation of pure phases of these materials [12]. The mean grain size ( $D$ ) of the particles was estimated from the XRD line broadening using the Scherrer equation [52]:

$$D = 0.89\lambda/\beta \cos \theta \quad (2)$$

where  $\lambda$  is the wavelength (Cu  $K_\alpha$ ),  $\beta$  is the full width at the half-maximum (FWHM) of the CuO and NiO lines, and  $\theta$  is the diffraction angle. Importantly, the annealing temperature was found to greatly affect the particle morphology of the as-prepared CuO and NiO powders.

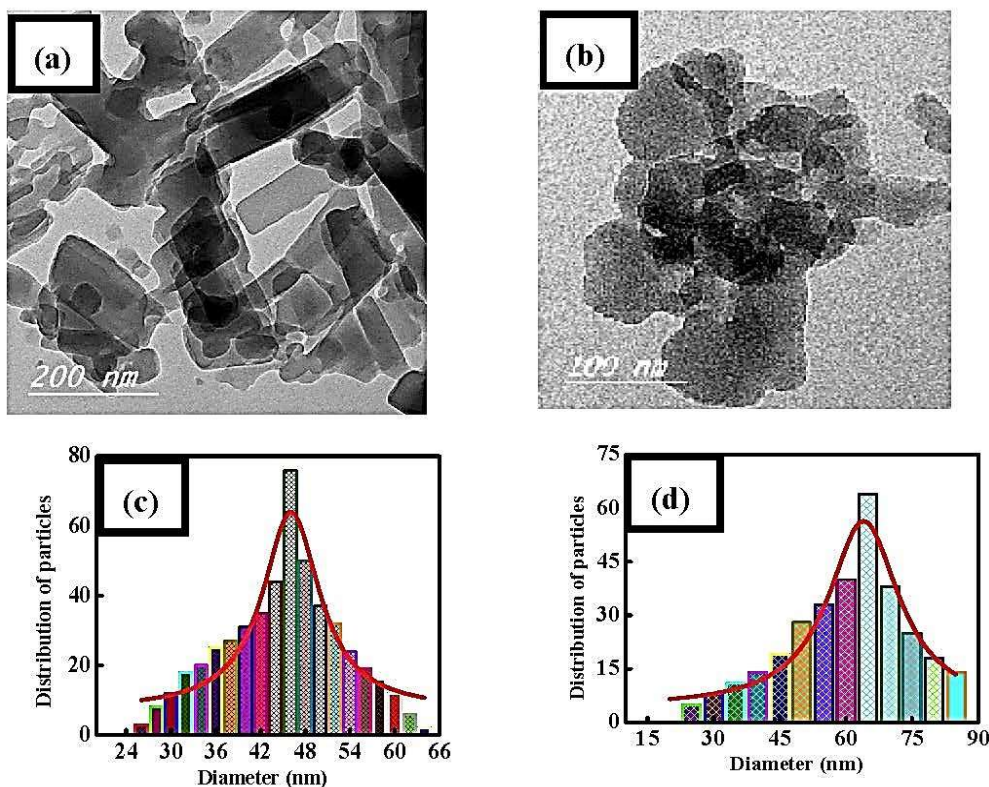


**Figure 2.** (a,b) Transmission electron microscopy (TEM) images of the ahpvCu and ahpvNi complexes, and (c,d) their calculated histograms, respectively.

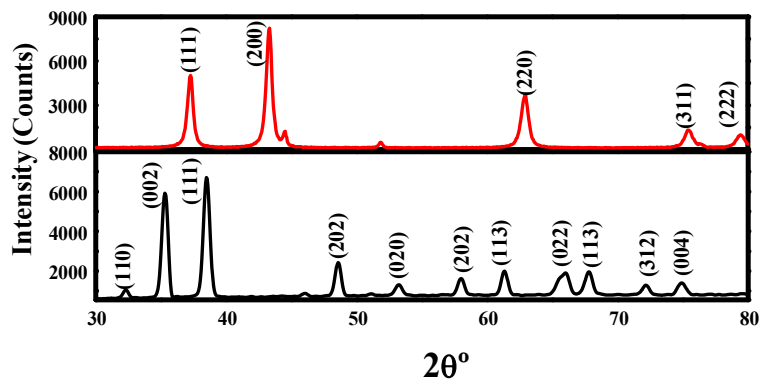


**Figure 3.** X-ray diffraction (XRD) patterns of the CuO (black) and NiO (red) nanoparticles.

### 2.8. Catalytic Oxidation of Benzyl Alcohol Using Schiff-Base M(II) Complexes and Their Oxides

The catalytic oxidation of BzOH in DMSO and other organic solvents was performed using the prepared nanosized Cu and Ni Schiff-base complexes (ahpvCu, ahpnCu, and ahpvNi) and their metal oxide (CuO and NiO) nanoparticles in the presence of aqueous H<sub>2</sub>O<sub>2</sub> as the oxidant under different experimental conditions, as described in Tables S4–S6. The obtained results clearly demonstrate that the prepared nanosized complexes and their MO exhibit efficient and highly selective catalytic oxidation of benzyl alcohol (BzOH) to the corresponding benzaldehyde (BzH) as the main product, compared to other conceptually and structurally related catalysts as illustrated in Table 2. This finding implied the crucial role of sonochemical approach in providing much higher surface area nanocatalysts compared to other conventional methods of synthesis.

**Table 2.** Comparison of the catalytic activity for BzOH oxidation using Schiff-base complexes and metal oxides.

Compound	Conversion (%)	Selectivity (%)
<sup>a</sup> ahpvCu	95	100
<sup>a</sup> ahpnbcu	94	100
<sup>b</sup> npisnphCu	79	100
<sup>b</sup> bsisnphCu	90	100
<sup>a</sup> CuO	96	100
<sup>c</sup> CuO	69	91

<sup>a</sup> This work, <sup>b</sup> Ref. [19], and <sup>c</sup> Ref. [21].

### 2.8.1. Effect of Temperature

The effect of temperature on the catalytic activity of the prepared Schiff base-M(II) (M = Cu and Ni) complexes and their metal oxides (MO) toward the oxidation of BzOH in DMSO, using aqueous H<sub>2</sub>O<sub>2</sub> as the oxygen source, was evaluated and optimized at different temperatures (60, 70, 80, and 90 °C) and time intervals. Tables S4 and S5 summarize the data obtained from using both ahpvCu and its corresponding CuO as catalysts presented in Figure 4. For all prepared nanocatalysts, gas chromatography (GC) confirmed that BzH was the solely generated product for BzOH oxidation reaction.

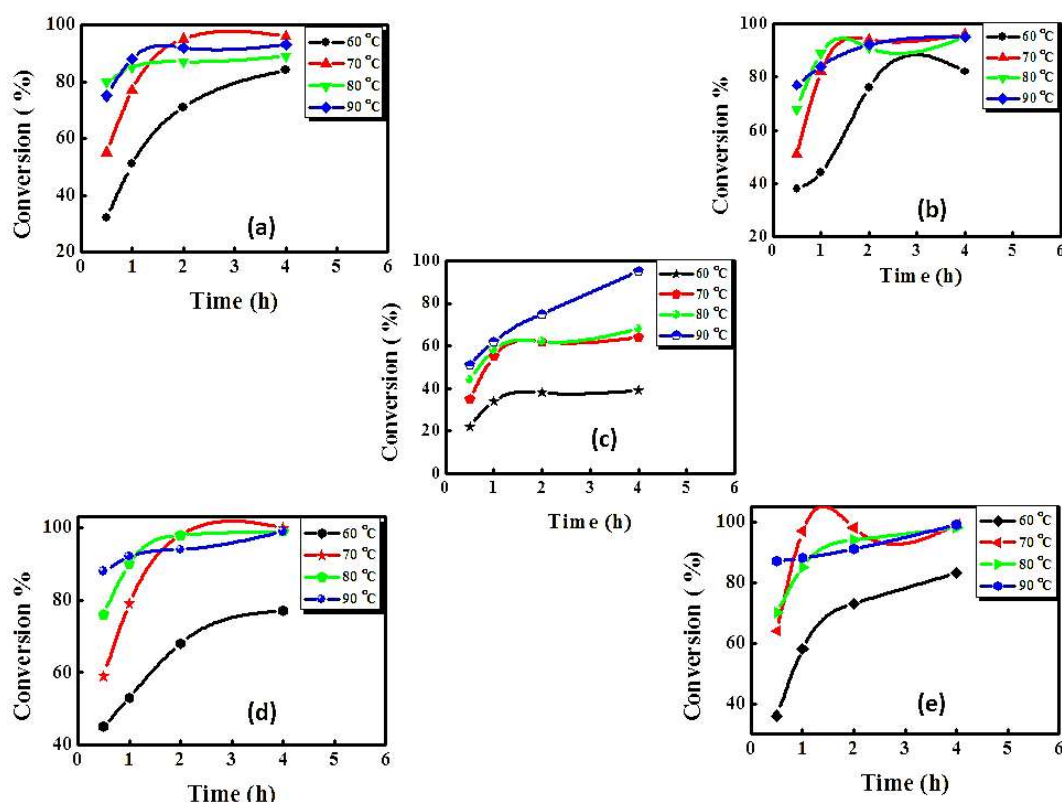


**Figure 4.** Oxidation of benzyl alcohol (1.0 mmol) catalyzed by the prepared Schiff base-M(II) complexes and their respective metal oxide (MO) (0.03 mmol) using aqueous H<sub>2</sub>O<sub>2</sub> (3.0 mmol) in dimethylsulfoxide (DMSO) at designated temperatures using: (a) ahpvCu, (b) ahpnbcu, (c) ahpvNi complexes, (d) CuO, and (e) NiO.

Control experiments using only H<sub>2</sub>O<sub>2</sub> (i.e., in the absence of the Schiff base-M(II) complexes or their MO) showed that no other carbonyl products were formed to a measurable extent under similar conditions. Importantly, as can be seen from Figure 4d,e, it is clearly established that the MOs exhibit higher catalytic activity toward BzOH oxidation than their parent complexes at all the investigated

temperatures [53]. In the case of CuO (Figure 4d), for instance, the rate of conversion is remarkably increased with the reaction temperature, meanwhile the selectivity toward BzH remained constant. According to the results shown in Table S5, after 30 min, the conversion of BzOH to BzH increased from 45% to 88% upon increasing the temperature from 60 to 90 °C, while the selectivity for generation of BzH was nearly 100% under both conditions.

### 2.8.2. Effect of the Solvent

Previous studies have shown that the nature of the solvent plays a crucial role in the catalytic oxidation of alcohols and the control of the stereo- and chemo-selectivity, as well as the conversion yield [19,54–56]. In the present study, the catalytic behavior of the prepared Schiff-base M(II) complexes and their MOs toward the oxidation of BzOH was investigated in various solvents, including acetonitrile (AN), acetone (AC), *N,N'*-dimethylformamide (DMF), and dimethylsulfoxide (DMSO). The catalytic reactions were conducted under the optimized conditions for all catalysts, and the obtained results are presented in Table 3. As can be seen from these data, the catalytic activity is prominently influenced by the nature of the solvent, with DMSO being the best solvent for all catalysts affording 94–98% conversion of BzOH into BzH. This is probably, due to the fact that DMSO is the most polar of all the studied solvents and has the greatest coordinating ability, which strongly activated the catalyst toward the oxidation of BzOH. Although NiO yielded 92–97% of BzH, its parent Ni-complex gave the lowest conversion (~55%). Therefore, under these conditions, the Schiff-base Cu-complexes are more efficient catalysts than their Ni-counterparts.

**Table 3.** Summary of the optimized parameters for oxidation of BzOH using the five prepared nanocatalysts.

Compound <sup>a</sup>	Solvent	Temp. (°C)	Time (h)	Yield (%)				Conversion (%)	Selectivity (%)
				BzH <sup>b</sup>	BzA <sup>c</sup>	Side Products	R		
ahpvCu	DMF	70	2	33	0	0	67	33	100
	Acetone			7	7	0	86	14	50
	DMSO			95	0	0	5	95	100
	Acetonitrile			48	0	0	52	48	100
ahpnbCu	DMF	70	2	44	0	0	56	44	100
	Acetone			25	11	0	64	36	69
	DMSO			94	0	0	6	94	100
	Acetonitrile			46	0	0	54	46	100
ahpvNi	DMF	70	1	15	0	0	85	15	100
	Acetone			5	4	3	88	12	42
	DMSO			55	0	0	45	55	100
	Acetonitrile			28	0	0	72	28	100
CuO	DMF	70	2	61	0	0	39	61	100
	Acetone			18	11	4	67	33	54
	DMSO			98	0	0	2	98	100
	Acetonitrile			66	0	0	34	66	100
NiO	DMF	70	1	52	0	0	48	52	100
	Acetone			45	12	0	43	57	79
	DMSO			97	0	0	3	97	100
	Acetonitrile			84	0	0	16	84	100

<sup>a</sup> Oxidation of benzyl alcohol (R) (1.0 mmol) catalyzed by ahpvCu complex (0.03 mmol) with aqueous H<sub>2</sub>O<sub>2</sub> (3.00 mmol) in 10 cm<sup>3</sup> DMSO for 0.5–4 h. <sup>b</sup> Yield based on gas chromatography (GC) results: Selectivity percentage of the target oxide product, benzaldehyde (BzH), and the other product, benzoic acid (BzA). <sup>c</sup> The side product was mainly benzoic acid (BzA).

In contrast to DMSO, all catalysts showed drastically poor catalytic activity when acetone was used as the solvent, with the highest selectivity (~69%) and conversion (~36%) for BzOH oxidation being achieved when ahpnbCu complex is used. In view of these results, it can be concluded that the most suitable solvent for the efficient catalytic oxidation of benzyl alcohol by the ahpvCu, ahpnbCu, and ahpvNi complexes, along with CuO and NiO, is DMSO, as previously reported [57].

### 2.8.3. Effect of the Catalyst Concentration

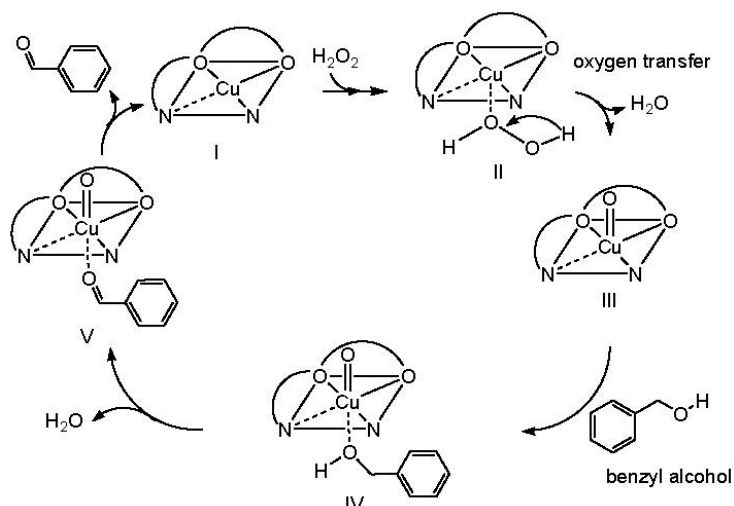
The amount of catalyst used for the oxidation of primary alcohols, such as benzyl alcohol has a profound impact on the kinetics and yield of the produced products, particularly benzaldehyde [17,19,56]. In this work, the effect of the catalyst concentration was probed by deliberately adding different molar ratios (0.01, 0.02, 0.03, and 0.04 mmol) of the three complexes (ahpvCu, ahpnCu, and ahpvNi) and their oxides (CuO and NiO) to a BzOH solution in DMSO in the presence of aqueous H<sub>2</sub>O<sub>2</sub>, while the other experimental parameters were kept at their optimum values. For all catalysts, the obtained results (Table S6) suggest that the catalytic activity is enhanced by increasing catalyst concentration from 0.01 to 0.03 mmol, while it decays at values greater than 0.04 mmol.

### 2.8.4. Mechanistic Aspects of the Catalytic Oxidation of Benzyl Alcohol

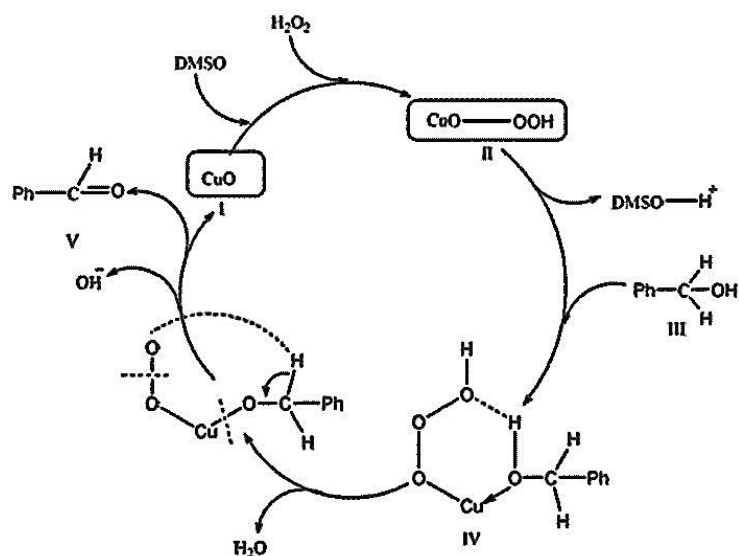
The data obtained for the five investigated nanocatalysts, under various experimental conditions, revealed several important features on the catalytic oxidation of BzOH. Firstly, the catalytic performance of the ahpvNi complex is markedly lower than that of both copper complexes (ahpvCu and ahpnCu). This behavior implies that oxygen transfer from H<sub>2</sub>O<sub>2</sub> to the catalyst is much easier in the case of the copper complexes than in the Ni congener, as previously reported for structurally-related systems [19,21,58,59]. Secondly, the catalytic activity of the MOs is greater than that of their parent Schiff-base complexes. This is explained by the fact that the oxides afford comparatively smaller-sized nanoparticles than the parent complexes, with consequently larger surface-to-volume ratios, thereby offering more efficient means for catalytic activity. Thirdly, in most catalytic processes, the major oxidation product was BzH and DMSO was found to be the best solvent for this catalytic oxidation reaction as both benzyl alcohol and the oxidant (H<sub>2</sub>O<sub>2</sub>) are soluble in it. Finally, from catalyst recovery viewpoint, the separation and/or recycling of MO nanoparticles from the reaction mixture upon completion of the catalytic reaction was successfully achieved at least 3 times and showed negligible decrease in their catalytic performance. Given their solubility in all employed organic solvents, the recovery of Schiff-based Cu- and Ni-complexes was not possible, as expected for homogeneous catalysis.

The catalytic activity of the prepared complexes correlates with their high stability in different solvents, which are able to accommodate the octahedral structure of ahpnCu and ahpvNi and tetrahedral geometry of ahpvCu (Scheme S1). In view of these proposed structures, the complexes contain open coordination sites for the oxidant (H<sub>2</sub>O<sub>2</sub>), thus replacing the H<sub>2</sub>O molecules and binding directly to the central cation (M<sup>2+</sup>). This allowed oxygen to be transferred from H<sub>2</sub>O<sub>2</sub> to M<sup>2+</sup> [19,58–60] (Scheme 1). This behavior can be detected spectroscopically (UV-Vis) by monitoring the changes in the characteristic peaks of each complex in DMSO at 70 °C, before and after addition of H<sub>2</sub>O<sub>2</sub>, as shown in Figures S4 and S5. Putatively, these spectral changes can be attributed to the substitution of H<sub>2</sub>O by H<sub>2</sub>O<sub>2</sub> molecules, as shown in the proposed mechanism in Scheme 1.

As for the catalytic oxidation of BzOH into BzH using MO nanoparticles (MO = CuO and NiO) catalysts, it is proposed that DMSO abstracts a proton (H<sup>+</sup>) from H<sub>2</sub>O<sub>2</sub> to generate a perhydroxyl anion (OOH<sup>-</sup>), which then combines with MO to yield MO–OOH. This species attacks BzOH to form peroxy-carboximidic acid intermediate (step IV in Scheme 2), which is then converted into BzH with concomitant regeneration of the catalyst. In view of the proposed mechanistic pathways for the catalytic oxidation of BzOH, it can be concluded that both the phenyl ring and OH group of benzyl alcohol may interact with the metal center of MO (M<sup>2+</sup>), whereas the inner active sites remain intact. However, the interaction of the phenyl ring and OH group with the outer metal ions of MO is also possible via adsorption of the phenyl ring on MO, as reported in ref. [56,61,62]. Importantly, the active sites of the catalyst can be regenerated by the oxidant. This leads to desorption of the desired product (BzH) molecules, thereby favoring the oxidation of BzOH to BzH. On this basis, it is likely that BzOH, DMSO, and H<sub>2</sub>O<sub>2</sub> interact efficiently with MO, affording the eventual formation of BzH, as described by step V in Scheme 2 [17,19,55].



**Scheme 1.** Proposed mechanism for the catalytic oxidation of benzyl alcohol by ahpnbcu.



**Scheme 2.** Proposed mechanism for the catalytic oxidation of benzyl alcohol by CuO.

### 3. Materials and Methods

#### 3.1. Chemicals

All solvents, chemicals, and starting materials utilized in this work, such as DMSO, DMF, acetone, acetonitrile, benzyl alcohol, 3-methoxysalicylaldehyde, 2-amino-3-hydroxypyridine, 4-nitrobenzaldehyde, copper acetate, nickel nitrate hexahydrate, hydrogen peroxide, manganese dioxide, and sodium sulfite were obtained from Sigma-Aldrich Chemie (Darmstadt, Germany), and used as received.

#### 3.2. Synthesis of Schiff-Base Ligands

The Schiff-base ligands were prepared, as shown in Scheme S2, by condensation of 3-methoxysalicylaldehyde (0.152 g, 1.0 mmol) or 4-nitrobenzaldehyde (0.151 g, 1.0 mmol) with 2-amino-3-hydroxypyridine (0.110 g, 1.0 mmol) in a 1:1 molar ratio in 10 mL of ethanol. The reaction mixtures were then refluxed for 1 h, after which the obtained solid precipitates were filtered off, rinsed with distilled water, dried, and then recrystallized from ethanol to afford an overall yield of 88–90%.

### 3.3. Preparation of Nanosized Cu- and Ni-Schiff Base Complexes via a Sonochemical Approach

An ethanolic solution (10 mL, 0.1 M) of the metal salts  $\text{Cu}(\text{CH}_3\text{COO})_2 \cdot \text{H}_2\text{O}$ , 0.199 g or  $\text{Ni}(\text{NO}_3)_2 \cdot 6\text{H}_2\text{O}$ , 0.291 g was placed in an ultrasonic probe operated at 24 kHz with a maximum force output of 400 W. A solution (10 mL, 0.1 M) of the Schiff base ahpv ligand (0.260 g) or 10 mL of a 0.2 M solution of the ahpnb ligand was added dropwise to the metal salt solution. The reaction mixture was then exposed to 10–15 min of sonochemical irradiation, allowing for nanoparticles formation of the desired complex. The obtained precipitate was filtered off, rinsed with ethanol, and then dried in air (yield: 72–84%). The proposed structures of the synthesized complexes are illustrated in Scheme S1.

### 3.4. Preparation of Nanosized NiO and CuO

NiO and CuO nanoparticles were prepared by calcination of 0.05 g of the ahpvCu, ahpvNi, and ahpnbCu complexes in air at 500 °C at a heating rate of 10 °C  $\text{min}^{-1}$ . The resulting MOs were washed with ethanol and dried in a desiccator. The MO structure was confirmed by TEM and XRD analyses.

### 3.5. Physical Measurements

The decomposition temperatures, as well as the melting point of the Schiff-base ligands, and corresponding complexes were determined using a Gallenkamp (London, UK) instrument. The IR spectra were recorded as KBr pellets of the compounds in the range of 4000–400  $\text{cm}^{-1}$  on a Shimadzu FTIR model 8101 spectrophotometer. Molar conductivity experiments were performed via a JENWAY conductivity meter model 4320 at 298 K using DMF as the solvent. UV-visible (UV-Vis) spectra of the compounds in DMF were recorded in a 10-mm quartz cell using a PG spectrophotometer model T+80.  $^1\text{H-NMR}$  spectra, in which tetramethylsilane (TMS) was used as internal standard ( $\delta$  ppm) and  $\text{DMSO-}d_6$  as the solvent were obtained through a BRUKER model 400 MHz. The C, H, and N elemental analysis of the Schiff-base ligands and their Ni(II) and Cu(II) complexes was carried out using a Perkin-Elmer (model 240 C) elemental analyzer (Mount Holly, NJ, USA). Magnetic measurements were conducted on a Gouy's balance and diamagnetic corrections were performed using Pascal's constants using  $\text{Hg}[\text{Co}(\text{SCN})_4]$  as a calibrant. Thermogravimetric testing was undertaken at a heating rate of 10 °C  $\text{min}^{-1}$  under  $\text{N}_2$  atmosphere using a Shimadzu corporation 60H analyzer (Kyoto, Japan). The value of the absorbance of a  $5 \times 10^{-3}$  M solution of each complex was recorded over wide range of pH values. The pH of a series of Britton–Robinson (BR) universal buffers was determined using a HANNA 211 pH meter at 298 K.

Transmission electron microscope (TEM-2100) at the Faculty of Science, Alex University was employed to obtain the TEM images of all prepared nanocatalysts. Ultrasonic irradiation was obtained via an ultrasonic generator (Dr. Hielscher UP400 S ultrasonic processor) prepared with an "H22" sonotrode of diameter 22 mm, working at 24 kHz at a maximum force output of 400 W. XRD measurements were performed using a Philips diffractometer with monochromatized  $\text{CuK}\alpha$  radiation. Image Launcher of the Broken Symmetry Software, version 1.4.3.6.7 was employed to determine the particle size distribution of the prepared Ni/Cu-complexes and their corresponding MOs.

### 3.6. Catalytic Oxidation Experiments

The catalytic oxidation of BzOH to the corresponding BzH by the nanosized Ni/Cu-Schiff base complexes and their NiO/CuO nanoparticles was studied in the presence of  $\text{H}_2\text{O}_2$ . In a typical reaction, BzOH (0.1 mL, 1.0 mmol) was added to a solution of the M(II) complex or metal oxide (0.03 mmol) in 10 mL of DMSO under stirring conditions at different temperatures (60, 70, 80, and 90 °C) in a water bath. The reaction was initiated by adding aqueous  $\text{H}_2\text{O}_2$  (30%) at each temperature and monitored by GC. The obtained oxidation products were identified by matching their retention times with those of authentic samples. Control experiments were conducted by treating a withdrawn sample (ca. 2 mL) of the reaction mixture with solid  $\text{MnO}_2$  (to quench the excess  $\text{H}_2\text{O}_2$ ) and then adding anhydrous  $\text{Na}_2\text{SO}_4$  (to absorb the excess water molecules) under the same conditions to those of the catalytic runs.

The resulting slurry was filtered off and the obtained filtrate was injected into the GC. This protocol allowed independent measurements for each sample. The amount of generated oxidation product (BzH) obtained upon chemical conversion of BzOH was calculated using computerized standard calibration curves.

#### 4. Conclusions

In this study, two Schiff-base ligands derived from the condensation of 2-amino-3-hydroxypyridine with 3-methoxysalicylaldehyde or 4-nitrobenzaldehyde were synthesized, and their nanosized Cu(II) and Ni(II) complexes, namely ahpvCu, ahpnbcu, and ahpvNi were obtained via a sonochemical approach. The results obtained by a wide range of structural tools revealed the formation of 1:1 (metal: ligand) complexes in the case of ahpvCu and ahpvNi, while a 1:2 stoichiometric ratio was found for the ahpnbcu congener. The prepared nanosized Schiff-base complexes, along with their MOs, exhibit excellent catalytic performance in the oxidation of BzOH to BzH, particularly when carried out in DMSO using H<sub>2</sub>O<sub>2</sub> as the oxidizing agent. The present finding makes the prepared complexes good candidates for the investigation of the catalytic conversions of other organic compounds and alcohols.

**Supplementary Materials:** The following are available online at <http://www.mdpi.com/2073-4344/8/10/452/s1>, Figures S1–S5: Electronic spectra, pH-profiles, TEM images, and repetitive scans for designated complexes and their MOs, Tables S1–S6: Physical and analytical properties, as well as IR and thermal analysis data for the ligands and their respective complexes along with data for catalytic oxidation of benzyl alcohol under various conditions. Schemes S1 and S2: Proposed structures and procedure for the prepared complexes.

**Author Contributions:** Conceptualization, L.H.A.R. and A.N.; Data curation, A.M.A.-D. and S.M.A.-F.; Formal analysis, T.M.A.; Investigation, S.M.A.-F. and A.M.A.; Methodology, A.M.A.-D. and A.N.; Project administration, T.M.A.; Resources, A.M.A.; Supervision, S.I.A.-S., L.H.A.R. and A.N.

**Acknowledgments:** We extend our sincere appreciation to the Deanship of Scientific Research at King Saud University for funding this project through Research Group (RG #236) and RSSU for their technical support. We also thank the Deanship of Scientific Research at Princess Nourah bint Abdulrahman University for funding of this work through Research Group (RGP-1438-0005).

**Conflicts of Interest:** The authors declare no conflict of interest.

#### References

1. Abdel-Rahman, L.H.; Abu-Dief, A.M.; El-Khatib, R.M.; Abdel-Fatah, S.M. Sonochemical synthesis, DNA binding, antimicrobial evaluation and in vitro anticancer activity of three new nano-sized Cu (II), Co (II) and Ni (II) chelates based on tri-dentate NOO imine ligands as precursors for metal oxides. *J. Photochem. Photobiol. B* **2016**, *162*, 298–308. [[CrossRef](#)] [[PubMed](#)]
2. Abdel-Rahman, L.H.; El-Khatib, R.M.; Nassr, L.A.; Abu-Dief, A.M.; Lashin, F.E.-D. Design, characterization, teratogenicity testing, antibacterial, antifungal and DNA interaction of few high spin Fe (II) Schiff base amino acid complexes. *Spectrochim. Acta Part A* **2013**, *111*, 266–276. [[CrossRef](#)] [[PubMed](#)]
3. Gupta, K.; Sutar, A.K. Catalytic activities of Schiff base transition metal complexes. *Coord. Chem. Rev.* **2008**, *252*, 1420–1450. [[CrossRef](#)]
4. Liu, X.; Manzur, C.; Novoa, N.; Celedón, S.; Carrillo, D.; Hamon, J.R. Multidentate unsymmetrically-substituted Schiff bases and their metal complexes: Synthesis, functional materials properties, and applications to catalysis. *Coord. Chem. Rev.* **2018**, *357*, 144–172. [[CrossRef](#)]
5. Türkkan, B.; Sariboğa, B.; Sariboğa, N. Synthesis, characterization and antimicrobial activity of 3,5-di-tert-butylsalicylaldehyde-S-methylthiosemicarbazones and their Ni (II) complexes. *Transit. Met. Chem.* **2011**, *36*, 679–684. [[CrossRef](#)]
6. Boghaei, D.M.; Mohebi, S. Synthesis, characterization and study of vanadyl tetradentate Schiff base complexes as catalyst in aerobic selective oxidation of olefins. *J. Mol. Catal. A Chem.* **2002**, *179*, 41–51. [[CrossRef](#)]
7. Cozzi, P.G. Metal-Salen Schiff base complexes in catalysis: Practical aspects. *Chem. Soc. Rev.* **2004**, *33*, 410–421. [[CrossRef](#)] [[PubMed](#)]

8. Kannan, S.; Ramesh, R. Synthesis, characterization, catalytic oxidation and biological activity of ruthenium (III) Schiff base complexes derived from 3-acetyl-6-methyl-2H-pyran-2,4-(3H)-dione. *Polyhedron* **2006**, *25*, 3095–3103. [[CrossRef](#)]
9. Wu, G.; Wang, X.; Guan, N.; Li, L. Palladium on graphene as efficient catalyst for solvent-free aerobic oxidation of aromatic alcohols: Role of graphene support. *Appl. Catal. B* **2013**, *136*, 177–185. [[CrossRef](#)]
10. Chevrot, C.; Henri, T. Electrosynthesis and oxidation of new oligoazomethines containing *N*-ethylcarbazole groups. *Synth. Met.* **2001**, *118*, 157–166. [[CrossRef](#)]
11. Tieke, B. Coordinative supramolecular assembly of electrochromic thin films. *Curr. Opin. Colloid Interface Sci.* **2011**, *16*, 499–507. [[CrossRef](#)]
12. Khalaji, A.D. Preparation and characterization of NiO nanoparticles via solid-state thermal decomposition of nickel (II) Schiff base complexes [Ni (salophen)] and [Ni (Me-salophen)]. *J. Clust. Sci.* **2013**, *24*, 209–215. [[CrossRef](#)]
13. Xu, H.; Xu, Z.F.; Yue, Z.Y.; Yan, P.F.; Wang, B.; Jia, L.W.; Li, G.M.; Sun, W.B.; Zhang, J.W. A novel deep blue-emitting Zn(II) complex based on carbazole-modified 2-(2-hydroxyphenyl) benzimidazole: Synthesis, bright electroluminescence, and substitution effect on photoluminescent, thermal, and electrochemical properties. *J. Phys. Chem. C* **2008**, *112*, 15517–15525. [[CrossRef](#)]
14. Ramesh, R. Spectral and catalytic studies of ruthenium (III) Schiff base complexes. *Inorg. Chem. Commun.* **2004**, *7*, 274–276. [[CrossRef](#)]
15. Bordoloi, A.; Sahoo, S.; Lefebvre, F.; Halligudi, S. Heteropoly acid-based supported ionic liquid-phase catalyst for the selective oxidation of alcohols. *J. Catal.* **2008**, *259*, 232–239. [[CrossRef](#)]
16. Maity, P.; Gopinath, C.S.; Bhaduri, S.; Lahiri, G.K. Applications of a high performance platinum nanocatalyst for the oxidation of alcohols in water. *Green Chem.* **2009**, *11*, 554–561. [[CrossRef](#)]
17. Mahdavi, V.; Mardani, M. Selective oxidation of benzyl alcohol with *tert*-butylhydroperoxide catalysed via Mn (II) 2,2-bipyridine complexes immobilized over the mesoporous hexagonal molecular sieves (HMS). *J. Chem. Sci.* **2012**, *124*, 1107–1115. [[CrossRef](#)]
18. Parmeggiani, C.; Cardona, F. Transition metal based catalysts in the aerobic oxidation of alcohols. *Green Chem.* **2012**, *14*, 547–564. [[CrossRef](#)]
19. Abdel-Rahman, L.H.; Abu-Dief, A.M.; Adam, M.S.S.; Hamdan, S.K. Some new nano-sized mononuclear Cu (II) Schiff base complexes: Design, characterization, molecular modeling and catalytic potentials in benzyl alcohol oxidation. *Catal. Lett.* **2016**, *146*, 1373–1396. [[CrossRef](#)]
20. Putla, S.; Amin, M.H.; Reddy, B.M.; Nafady, A.; Al Farhan, K.A.; Bhargava, S.K. MnO<sub>x</sub> Nanoparticle-Dispersed CeO<sub>2</sub> Nanocubes: A Remarkable Heteronanostructured System with Unusual Structural Characteristics and Superior Catalytic Performance. *ACS Appl. Mater. Interfaces* **2015**, *7*, 16525–16535. [[CrossRef](#)] [[PubMed](#)]
21. Poreddy, R.; Engelbrekt, C.; Riisager, A. Copper oxide as efficient catalyst for oxidative dehydrogenation of alcohols with air. *Catal. Sci. Technol.* **2015**, *5*, 2467–2477. [[CrossRef](#)]
22. Bhanage, B.M.; Fujita, S.-I.; Ikushima, Y.; Arai, M. Synthesis of dimethyl carbonate and glycols from carbon dioxide, epoxides, and methanol using heterogeneous basic metal oxide catalysts with high activity and selectivity. *Appl. Catal. A* **2001**, *219*, 259–266. [[CrossRef](#)]
23. Wachs, I.E. Recent conceptual advances in the catalysis science of mixed metal oxide catalytic materials. *Catal. Today* **2005**, *100*, 79–94. [[CrossRef](#)]
24. Choudhary, V.R.; Mondal, K.C. CO<sub>2</sub> reforming of methane combined with steam reforming or partial oxidation of methane to syngas over NdCoO<sub>3</sub> perovskite-type mixed metal-oxide catalyst. *Appl. Energy* **2006**, *83*, 1024–1032. [[CrossRef](#)]
25. Li, J.; Chang, H.; Ma, L.; Hao, J.; Yang, R.T. Low-temperature selective catalytic reduction of NO<sub>x</sub> with NH<sub>3</sub> over metal oxide and zeolite catalysts—A review. *Catal. Today* **2011**, *175*, 147–156. [[CrossRef](#)]
26. Zhang, M.; De Respinis, M.; Frei, H. Time-resolved observations of water oxidation intermediates on a cobalt oxide nanoparticle catalyst. *Nat. Chem.* **2014**, *6*, 362–367. [[CrossRef](#)] [[PubMed](#)]
27. Jampaiah, D.; Ippolito, S.J.; Sabri, Y.M.; Tardio, J.; Selvakannan, P.; Nafady, A.; Reddy, B.M.; Bhargava, S.K. Ceria-zirconia modified MnO<sub>x</sub> catalysts for gaseous elemental mercury oxidation and adsorption. *Catal. Sci. Technol.* **2016**, *6*, 1792–1803. [[CrossRef](#)]
28. Gervasini, A.; Auroux, A. Acidity and basicity of metal oxide surfaces II. Determination by catalytic decomposition of isopropanol. *J. Catal.* **1991**, *131*, 190–198. [[CrossRef](#)]

29. Lavalley, J. Infrared spectrometric studies of the surface basicity of metal oxides and zeolites using adsorbed probe molecules. *Catal. Today* **1996**, *27*, 377–401. [[CrossRef](#)]
30. Martin, D.; Duprez, D. Mobility of surface species on oxides. 1. Isotopic exchange of  $^{18}\text{O}_2$  with  $^{16}\text{O}$  of  $\text{SiO}_2$ ,  $\text{Al}_2\text{O}_3$ ,  $\text{ZrO}_2$ ,  $\text{MgO}$ ,  $\text{CeO}_2$ , and  $\text{CeO}_2\text{-Al}_2\text{O}_3$ . Activation by noble metals. Correlation with oxide basicity. *J. Phys. Chem.* **1996**, *100*, 9429–9438. [[CrossRef](#)]
31. Watanabe, M.; Osada, M.; Inomata, H.; Arai, K.; Kruse, A. Acidity and basicity of metal oxide catalysts for formaldehyde reaction in supercritical water at 673 K. *Appl. Catal. A* **2003**, *245*, 333–341. [[CrossRef](#)]
32. Arico, A.S.; Bruce, P.; Scrosati, B.; Tarascon, J.-M.; Van Schalkwijk, W. Nanostructured materials for advanced energy conversion and storage devices. *Nat. Mater.* **2005**, *4*, 366–377. [[CrossRef](#)] [[PubMed](#)]
33. Whitesides, G.M. Nanoscience, nanotechnology, and chemistry. *Small* **2005**, *1*, 172–179. [[CrossRef](#)] [[PubMed](#)]
34. Yu, B.; Meyyappan, M. Nanotechnology: Role in emerging nanoelectronics. *Solid-State Electron.* **2006**, *50*, 536–544. [[CrossRef](#)]
35. Guo, Y.G.; Hu, J.S.; Wan, L.J. Nanostructured materials for electrochemical energy conversion and storage devices. *Adv. Mater.* **2008**, *20*, 2878–2887. [[CrossRef](#)]
36. Somorjai, G.A.; Park, J.Y. Colloid science of metal nanoparticle catalysts in 2D and 3D structures. Challenges of nucleation, growth, composition, particle shape, size control and their influence on activity and selectivity. *Top. Catal.* **2008**, *49*, 126–135. [[CrossRef](#)]
37. Kandjani, A.E.; Sabri, Y.M.; Periasamy, S.R.; Zohora, N.; Amin, M.H.; Nafady, A.; Bhargava, S.K. Controlling core/shell formation of nanocubic p-Cu<sub>2</sub>O/n-ZnO toward enhanced photocatalytic performance. *Langmuir* **2015**, *31*, 10922–10930. [[CrossRef](#)] [[PubMed](#)]
38. Gottlieb, H.E.; Kotlyar, V.; Nudelman, A. NMR chemical shifts of common laboratory solvents as trace impurities. *J. Org. Chem.* **1997**, *62*, 7512–7515. [[CrossRef](#)] [[PubMed](#)]
39. Sharma, V.; Srivastava, A.; Srivastava, S. Synthetic, structural and antifungal studies of coordination compounds of Ru (III), Rh (III) and Ir (III) with tetradentate Schiff bases. *J. Serb. Chem. Soc.* **2006**, *71*, 917–928. [[CrossRef](#)]
40. Nakamoto, K. Infrared and Raman spectra of inorganic and coordination compounds. In *Part B: Applications in Coordination, Organometallic, and Bioinorganic Chemistry*, 6th ed.; John Wiley and Sons Inc.: Hoboken, NJ, USA, 2009.
41. Agarwal, S.K. Synthesis and characterization of some mixed ligand complexes of Pd (II), Rh (III) and Pt (IV) with carboxylic hydrazones as primary and dithiooxamide as co-ligand. *Asian J. Chem.* **2007**, *19*, 2581–2585.
42. Vatsa, G.; Pandey, O.; Sengupta, S. Synthesis, spectroscopic and toxicity studies of titanocene chelates of isatin-3-thiosemicarbazones. *Bioinorg. Chem. Appl.* **2005**, *3*, 151–160. [[CrossRef](#)] [[PubMed](#)]
43. Kusanur, R.A.; Ghate, M.; Kulkarni, M.V. Synthesis of *spiro*[indolo-1,5-benzodiazepines] from 3-acetyl coumarins for use as possible antianxiety agents. *J. Chem. Sci.* **2004**, *116*, 265–270. [[CrossRef](#)]
44. Silverstein, R.M.; Webster, F.X.; Kiemle, D.J.; Bryce, D.L. *Spectrometric Identification of Organic Compounds*, 8th ed.; John Wiley & Sons: Hoboken, NJ, USA, 2014; pp. 71–125. ISBN 978-0-470-61637-6.
45. Labisbal, E.; Sousa, A.; Castiñeiras, A.; García-Vázquez, J.A.; Romero, J.; West, D.X. Spectral and structural studies of metal complexes of isatin 3-hexamethyleneiminylthiosemicarbazone prepared electrochemically. *Polyhedron* **2000**, *19*, 1255–1262. [[CrossRef](#)]
46. Al-Maydama, H.; El-Shekeil, A.; Khalid, M.; Al-Karbouly, A. Thermal degradation behaviour of some polydithiooxamide metal complexes. *Eletica Quím.* **2006**, *31*, 45–52. [[CrossRef](#)]
47. Montazerzohori, M.; Jahromi, S.M.; Naghiha, A. Thermal analyses data and antimicrobial screening of some new nano-structure five coordinated cadmium complexes. *J. Ind. Eng. Chem.* **2015**, *22*, 248–257. [[CrossRef](#)]
48. Diefallah, E.-H.M. Kinetic analysis of thermal decomposition reactions: Part VI. Thermal decomposition of manganese (II) acetate tetrahydrate. *Thermochim. Acta* **1992**, *202*, 1–16. [[CrossRef](#)]
49. Carmody, W.R. Demonstrating Job's method with colorimeter or spectrophotometer. *J. Chem. Educ.* **1964**, *41*, 615–616. [[CrossRef](#)]
50. Türkel, N. Stability constants of mixed ligand complexes of nickel (II) with adenine and some amino acids. *Bioinorg. Chem. Appl.* **2015**. [[CrossRef](#)] [[PubMed](#)]
51. Parrish, W. X-Ray powder diffraction analysis film and Geiger counter techniques. *Science* **1949**, *110*, 368–371. [[CrossRef](#)] [[PubMed](#)]

52. Scherrer, P. Bestimmung der Grösse und der Inneren Struktur von Kolloidteilchen Mittels Röntgenstrahlen, Nachrichten von der Gesellschaft der Wissenschaften. *Göttingen. Mathematisch-Physikalische Klasse* **1918**, *2*, 98–100.
53. Adam, M.S.S. Catalytic potentials of homodioxo-bimetallic dihydrazone complexes of uranium and molybdenum in a homogeneous oxidation of alkenes. *Monatsh. Chem.* **2015**, *146*, 1823–1836. [[CrossRef](#)]
54. Monfared, H.H.; Bikas, R.; Mayer, P. Homogeneous green catalysts for olefin oxidation by mono oxovanadium (V) complexes of hydrazone Schiff base ligands. *Inorg. Chim. Acta* **2010**, *363*, 2574–2583. [[CrossRef](#)]
55. Ragupathi, C.; Vijaya, J.J.; Kennedy, L.J. Synthesis, characterization of nickel aluminate nanoparticles by microwave combustion method and their catalytic properties. *Mater. Sci. Eng. B* **2014**, *184*, 18–25. [[CrossRef](#)]
56. Ragupathi, C.; Vijaya, J.J.; Narayanan, S.; Jesudoss, S.; Kennedy, L.J. Highly selective oxidation of benzyl alcohol to benzaldehyde with hydrogen peroxide by cobalt aluminate catalysis: A comparison of conventional and microwave methods. *Ceram. Int.* **2015**, *41*, 2069–2080. [[CrossRef](#)]
57. Noshiranzadeh, N.; Bikas, R.; Ślepokura, K.; Mayeli, M.; Lis, T. Synthesis, characterization and catalytic activity of new Cr (III) complex in oxidation of primary alcohols to aldehydes. *Inorg. Chim. Acta* **2014**, *421*, 176–182. [[CrossRef](#)]
58. Enamullah, M.; Islam, M.K. Syntheses, spectroscopy, optical properties, and diastereoselectivity of copper(II)-complexes with chiral aminoalcohol based Schiff bases. *J. Coord. Chem.* **2013**, *66*, 4107–4118. [[CrossRef](#)]
59. Zueva, E.; Walton, P.H.; McGrady, J.E. Catalytic alcohol oxidation by an unsymmetrical 5-coordinate copper complex: Electronic structure and mechanism. *Dalton Trans.* **2006**, 159–167. [[CrossRef](#)] [[PubMed](#)]
60. Banu, K.S.; Chattopadhyay, T.; Banerjee, A.; Bhattacharya, S.; Zangrando, E.; Das, D. Catechol oxidase activity of dinuclear copper (II) complexes of Robson type macrocyclic ligands: Syntheses, X-ray crystal structure, spectroscopic characterization of the adducts and kinetic studies. *J. Mol. Catal. A* **2009**, *310*, 34–41. [[CrossRef](#)]
61. Ma, C.Y.; Cheng, J.; Wang, H.L.; Hu, Q.; Tian, H.; He, C.; Hao, Z.P. Characteristics of Au/HMS catalysts for selective oxidation of benzyl alcohol to benzaldehyde. *Catal. Today* **2010**, *158*, 246–251. [[CrossRef](#)]
62. Ma, L.; Zhang, Q.; Cheng, L.; Wu, Z.; Yang, J. DFT studies on the mechanism of veratryl alcohol oxidation catalyzed by Cu-phen complexes. *RSC Adv.* **2014**, *4*, 30558–30565. [[CrossRef](#)]



© 2018 by the authors. Licensee MDPI, Basel, Switzerland. This article is an open access article distributed under the terms and conditions of the Creative Commons Attribution (CC BY) license (<http://creativecommons.org/licenses/by/4.0/>).